communications earth & environment

Article

https://doi.org/10.1038/s43247-024-01620-3

Strong persistent cooling of the stratosphere after the Hunga eruption

Check for updates

Matthias Stocker [1] ✉, Andrea K. Steiner [1], Florian Ladstädter [1], Ulrich Foelsche [1,2] & William J. Randel [3]

The 2022 eruption of the Hunga volcano was a major event that propelled aerosols and water vapor up to an altitude of 53–57 km. It caused an unprecedented stratospheric hydration that is expected to affect composition, thermal structure, circulation and dynamics for years. Using vertically high resolved satellite observations from radio occultation, we focus on the temperature impact in the stratosphere from the eruption in January 2022 until December 2023. Separating the signals of the Hunga eruption from the broader stratospheric variability reveals a strong persistent radiative cooling of up to –4 K in the tropical and subtropical middle stratosphere from early after the eruption until mid-2023, clearly corresponding to the water vapor distribution. Our results provide new insights from observations into both the localized temperature changes and the persistent stratospheric cooling caused by the Hunga eruption and document this exceptional climatic effect not seen for previous volcanic eruptions.

Temperature variability in the stratosphere is governed by a variety of different drivers, including changes in solar radiation, radiatively active species such as ozone and greenhouse gases, and also strong natural modes of variability such as the Quasi-Biennial Oscillation (QBO) and the Brewer-Dobson Circulation (BDC)[1]. Extreme events such as large wildfires[2,3], sudden stratospheric warmings[4] and volcanic eruptions[5–7], however, can also have profound and longer-lasting effects on stratospheric temperature, composition and dynamics. While well-documented large eruptions such as El Chichón in 1982 and Pinatubo in 1991 have shown significant impacts, the eruption of the Hunga volcano in the southern Pacific Ocean (20.5°S, 175.4°W) in mid-January 2022 represented an unprecedented event that differs significantly from previous large volcanic eruptions[8,9].

The eruption set a new record for the height of the volcanic plume and sent aerosols and trace gases to altitudes of up to 57 km[8,10]. The emission of sulfur dioxide (SO_2) was initially estimated at about 0.4–0.5 Tg[10,11] and later assumed to be 1.5 Tg[12], which is comparable to a rather small volcanic eruption. However, the SO_2 was rapidly converted to sulfate aerosol particles, resulting in a Stratospheric Aerosol Optical Depth (SAOD) anomaly not seen since the Pinatubo eruption[13–15].

As a submarine eruption, Hunga also injected substantial amounts of water vapor directly into the stratosphere, resulting in unprecedented stratospheric hydration[10,16]. Observational data from the Microwave Limb Sounder (MLS) indicate water vapor mixing ratios of up to 350 ppmv, while Radio Occultation (RO) profiles even show local mixing ratios exceeding 1000 ppmv (up to 3500 ppmv in some places) at about 25–35 km altitude[17]. These values are way above the stratospheric background values of about 5 ppmv, underlining this extraordinary behavior[10,17]. This injection of water vapor led to a significant global increase in stratospheric water content of about 8 to 13%[10,13,17].

The aerosol and water vapor plumes began to separate over time due to gravitational sedimentation of the aerosol plume in the Southern Hemisphere stratosphere and the rise of the water vapor plume with the ascending branch of the BDC, mainly confined between 35°S and 20°N during the first months after the eruption[12,18,19].

The SAOD perturbation by the aerosol plume almost reached pre-eruption levels within roughly 2 years while the water vapor is expected to persist in the stratosphere for up to 10 years since there are no considerable water vapor sinks in the stratosphere[13].

The eruption has had a significant and lasting impact on the composition and dynamics of the global stratosphere, particularly in the Southern Hemisphere[20,21]. This makes it one of the most significant climatic events in recent decades[13,22] also affecting global surface temperatures by causing a net positive radiative forcing[10,23]. In the stratosphere the changes include potential radiative cooling due to increased water vapor levels as well as shifts in stratospheric ozone levels and related trace gases[20,21,24,25].

Recent model and observational studies have indeed already shown remarkable changes in stratospheric dynamics, composition and temperature associated with the eruption for the first months after the event[18–20,24–26]. Some of these studies have already found evidence of strong stratospheric

[1]Wegener Center for Climate and Global Change, University of Graz, Graz, Austria. [2]Department of Astrophysics and Geophysics, Institute of Physics, University of Graz, Graz, Austria. [3]National Center for Atmospheric Research (NCAR), Boulder, CO, USA. ✉e-mail: matthias.stocker@uni-graz.at

temperature signatures associated with the Hunga eruption but focused predominantly on the temperature impacts within the first few months after the eruption and/or on specific latitudes or limited time intervals, using absolute temperature data and model simulations[18,24–26].

Our research extends these results and the framework by examining the longer-term impacts of the Hunga eruption on the stratosphere over a period of almost 2 years, from the eruption to December 2023. We use high-resolution satellite data to analyze the observed temperature changes in the stratosphere and separate the signals from the general stratospheric variability. Our study provides new insights into the regional and vertical changes in the temperature structure and evaluates the lasting impacts of the eruption on the stratospheric climate.

Results

We use satellite-based observations of Global Navigation Satellite System (GNSS) RO temperature[27,28] along with temperature and water vapor measurements from the MLS instrument[29–31] to monitor the Hunga plume's development and related temperature signals. Our goal is to trace the plume evolution and accurately assess its longer lasting impacts on the stratospheric temperature structure.

Temperature structures within the early post-eruption plume

The Hunga eruption injected a considerable amount of water vapor into the stratosphere, reaching up to an altitude of about 53 km[10]. Figure 1a shows that the maximum water vapor is found around an altitude of

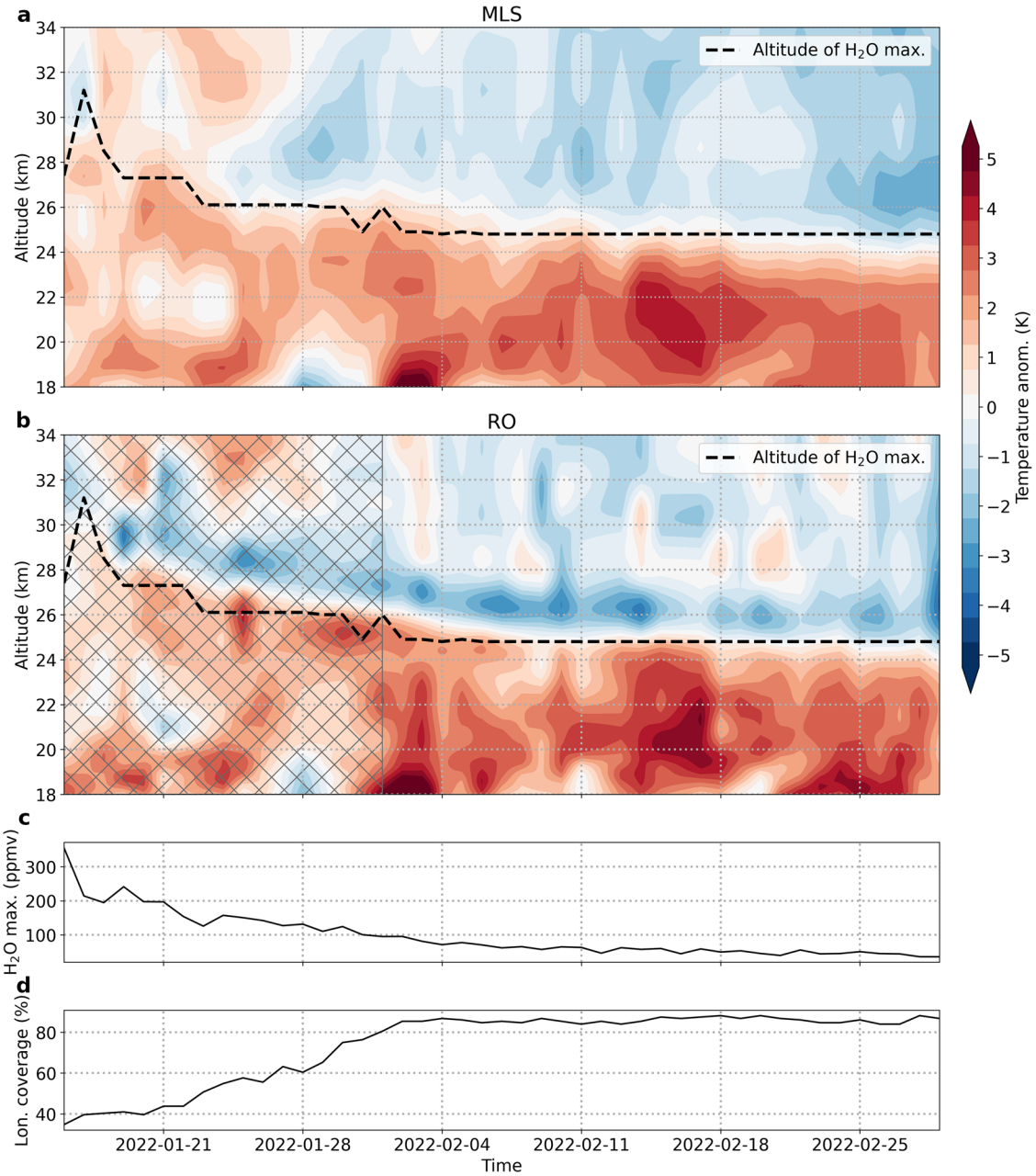

Fig. 1 | Temperature anomalies within the early post-eruption plume. MLS (**a**) and RO (**b**) temperature anomaly profiles recorded following the center of the early water vapor plume after the eruption on January 15 until end of February 2022. The hatched area in (**b**) displays where RO signals overestimate the cooling due to localized high water vapor mixing ratios. The dashed black line in (**a**) and (**b**) represents the height of the maximum water vapor mixing ratio from MLS. **c** shows the evolution of the maximum water vapor mixing ratio, **d** shows the estimated longitudinal extent of the water vapor plume in percent within the latitude region from 40°S to 25°N.

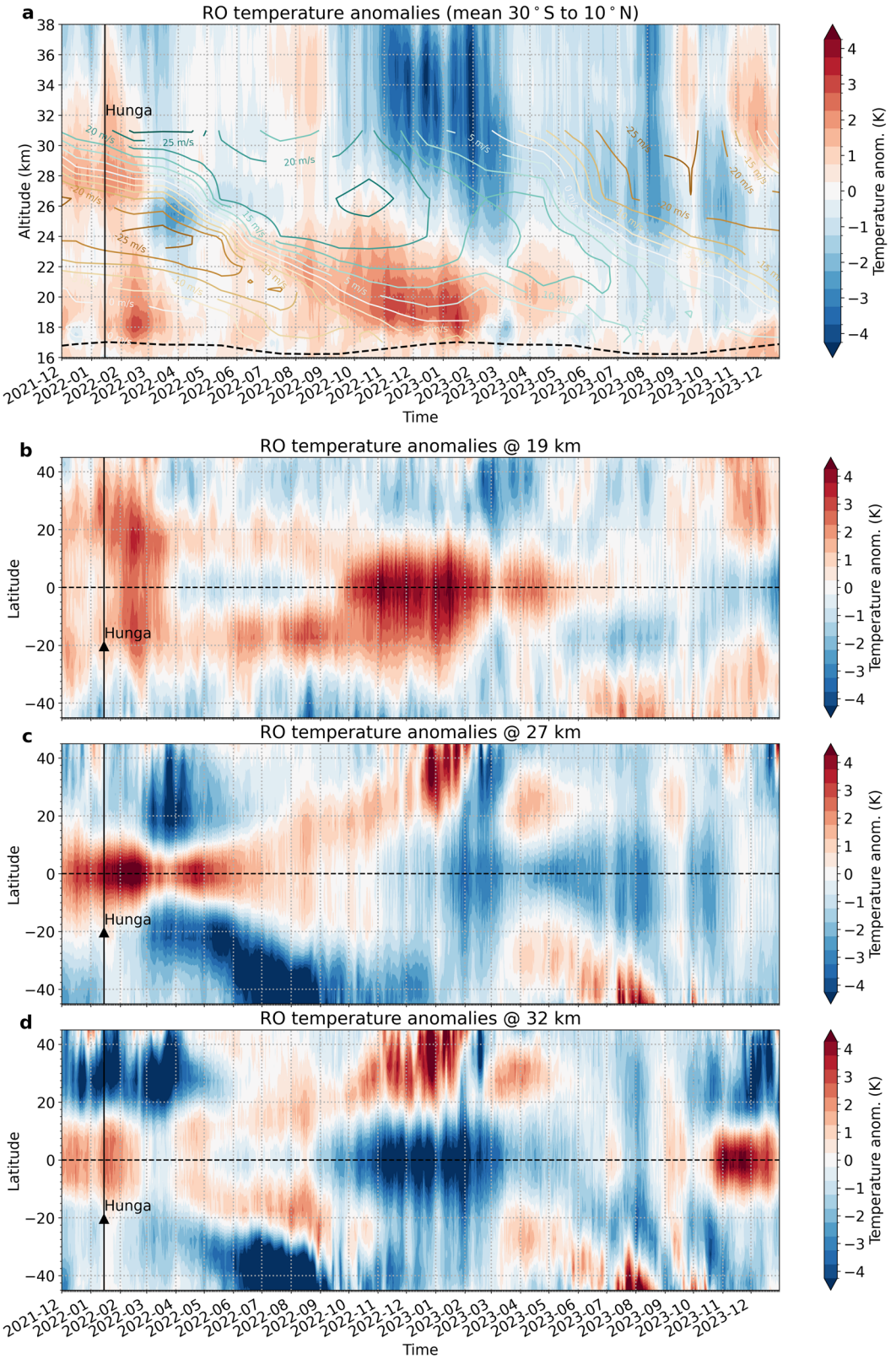

Fig. 2 | Daily temperature anomalies until 2 years after the Hunga eruption. Daily RO temperature anomalies from December 2021 to December 2023 are shown for the zonal mean 30°S to 10°N as function of altitude (**a**) as well as latitude-time slices at 19 km altitude (**b**), at 27 km altitude (**c**), and at 32 km altitude (**d**). Vertical lines mark the date of the eruption. The dashed black line in (**a**) indicates the climatological lapse-rate tropopause. The contour lines in the top panel show the Singapore wind anomalies (m s^{-1}) as indicator for the QBO, where positive anomalies (green lines) correspond to easterly winds and negative anomalies to westerly winds (brown lines).

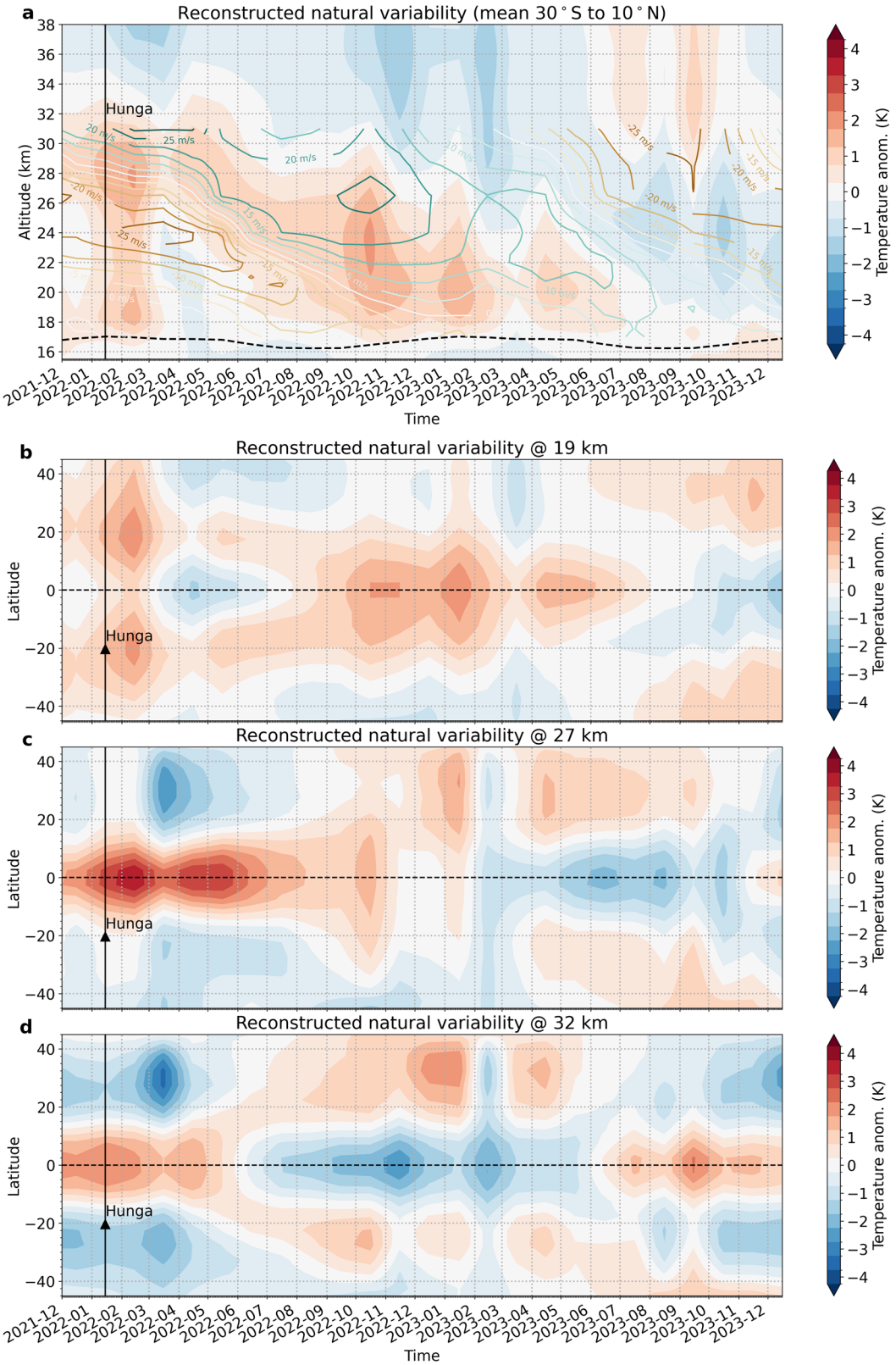

Fig. 3 | Reconstructed temperature anomalies from the natural variability modes. Reconstructed daily RO temperature anomalies derived from multiple linear regression analysis attributable to QBO, ENSO, solar flux and dynamical coupling with the high latitudes. The reconstructed anomalies are shown from December 2021 to December 2023 for the zonal mean 30°S to 10°N as function of altitude (**a**) as well as latitude-time slices at 19 km altitude (**b**), at 27 km altitude (**c**), and at 32 km altitude (**d**). Vertical lines mark the date of the eruption. The dashed black line in (**a**) indicates the climatological lapse-rate tropopause. The contour lines in the top panel show the Singapore wind anomalies (m s^{-1}) as indicator for the QBO, where positive anomalies (green lines) correspond to easterly winds and negative anomalies to westerly winds (brown lines).

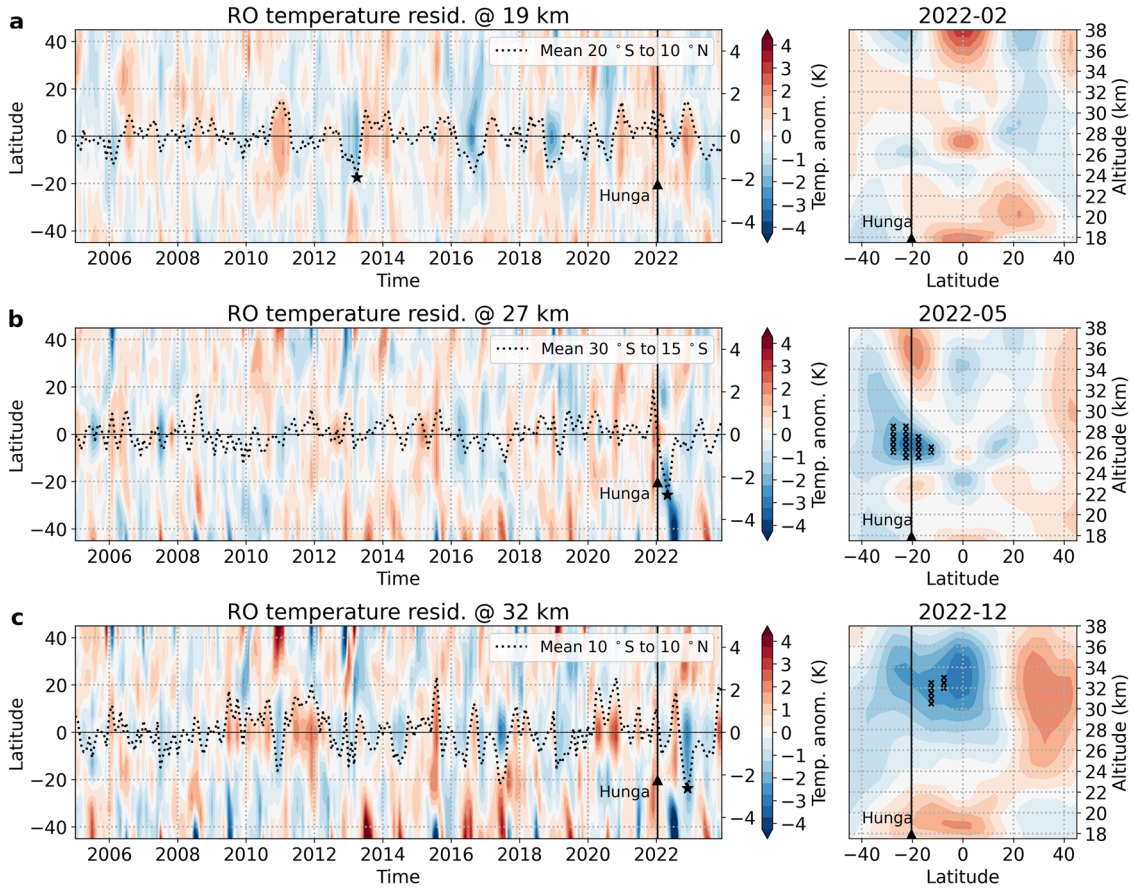

Fig. 4 | Monthly mean residual temperature anomalies. Zonal mean monthly RO residual temperature anomalies from January 2005 to December 2023 at 19 km (**a**), 27 km (**b**), and 32 km (**c**) after subtracting QBO/ENSO and high latitude variability. The dashed lines represent the mean over specific latitudes (**a**: 20°S to 10°N, **b**: 30°S to 15°S, **c**: 10°S to 10°N). The scale on the right-hand side of (**a**–**c**) represents the temperature scale for the dashed lines. The star symbols mark the strongest anomalies in the time series. The corresponding panels on the right side in (**a**–**c**) show altitude-latitude cross-sections for the months with the strongest anomalies, except for (**a**) where the strongest anomaly is found before the Hunga eruption. Anomalies in the right panels of (**a**–**c**) that are larger than three standard deviations are indicated with an X mark.

30 km in the following days, indicating a descent of the plume due to radiative cooling[14]. Within the first 3–4 weeks after the eruption, the plume evolved from a localized to a widespread distribution covering almost 90% of the globe longitudinally (Fig. 1d). We estimate the longitudinal extent by calculating the mean for the lower stratosphere (19–34 km) within the latitudinal region from 40°S to 25°N and considering longitudes that deviated by more than three standard deviations from the water vapor climatological mean. Notably, previous studies have shown that at least parts of the plume circumnavigated the globe within only 2 weeks[10]. In the same period the maximum MLS water vapor mixing ratio decreased from more than 300 ppmv to 30 ppmv (Fig. 1c). While the water vapor plume covered most of the stratosphere shortly after the eruption[10], the water vapor maximum derived from the MLS data gradually descended from its initial height to about 25 km (Fig. 1a, b).

During this descent in January and February, a temperature dipole structure following the altitudinal evolution of the water vapor plume[26] is clearly visible in temperature anomalies co-located with the plume (Fig. 1a, b). Anomalies are calculated with respect to the climatological temperature (from 2005 to 2021) at the given location for the corresponding month (c.f. section "Data and methods").

A cooling of about −3 K above the altitude of the water vapor maximum and a warming below is observable. The negative temperature anomaly as well as the radiatively driven plume descent[14] can be attributed to cooling driven by the presence of water vapor, while the observed warming can partly be explained by the greenhouse gas effect of water vapor affecting upwelling longwave radiation[14,19].

As, during this early phase, the water vapor plume overlaps with the aerosol plume[12] a radiative heating due to the presence of aerosols is also discussed, at least as far as the positive anomalies in the lowermost stratosphere are concerned[14,18]. Although aerosol and greenhouse gas effects are plausible, they likely affect only a limited altitude region.

Hours after the eruption, strong irregularities in bending angle[32] and temperature can be observed in RO profiles recorded within the volcanic plume (Fig. S1). However, it is important to note that the RO signals immediately post-eruption are strongly influenced by the presence of the huge amount of water vapor (see section "Data and methods"). It is estimated that a water vapor mixing ratio of 1500 ppmv corresponds to a "fictional" temperature anomaly of about –8 K[17]. Such localized high water vapor mixing ratios therefore cause an overestimation of the cooling in RO profiles until approximately early February as indicated by the shading in Fig. 1b.

However, rapid dispersal and diffusion of the water vapor plume starts soon after the eruption[10] and the direct effect on RO becomes negligible. This is confirmed by closely matching temperature patterns between RO and MLS (Fig. 1b vs. Fig. 1a). Also, model simulations[14] and radiosonde measurements[26] show a dipole structure in regions with increased water vapor shortly after the eruption. Since MLS averages over a broad altitude region and RO has a high vertical resolution, RO exhibits a more detailed vertical structure.

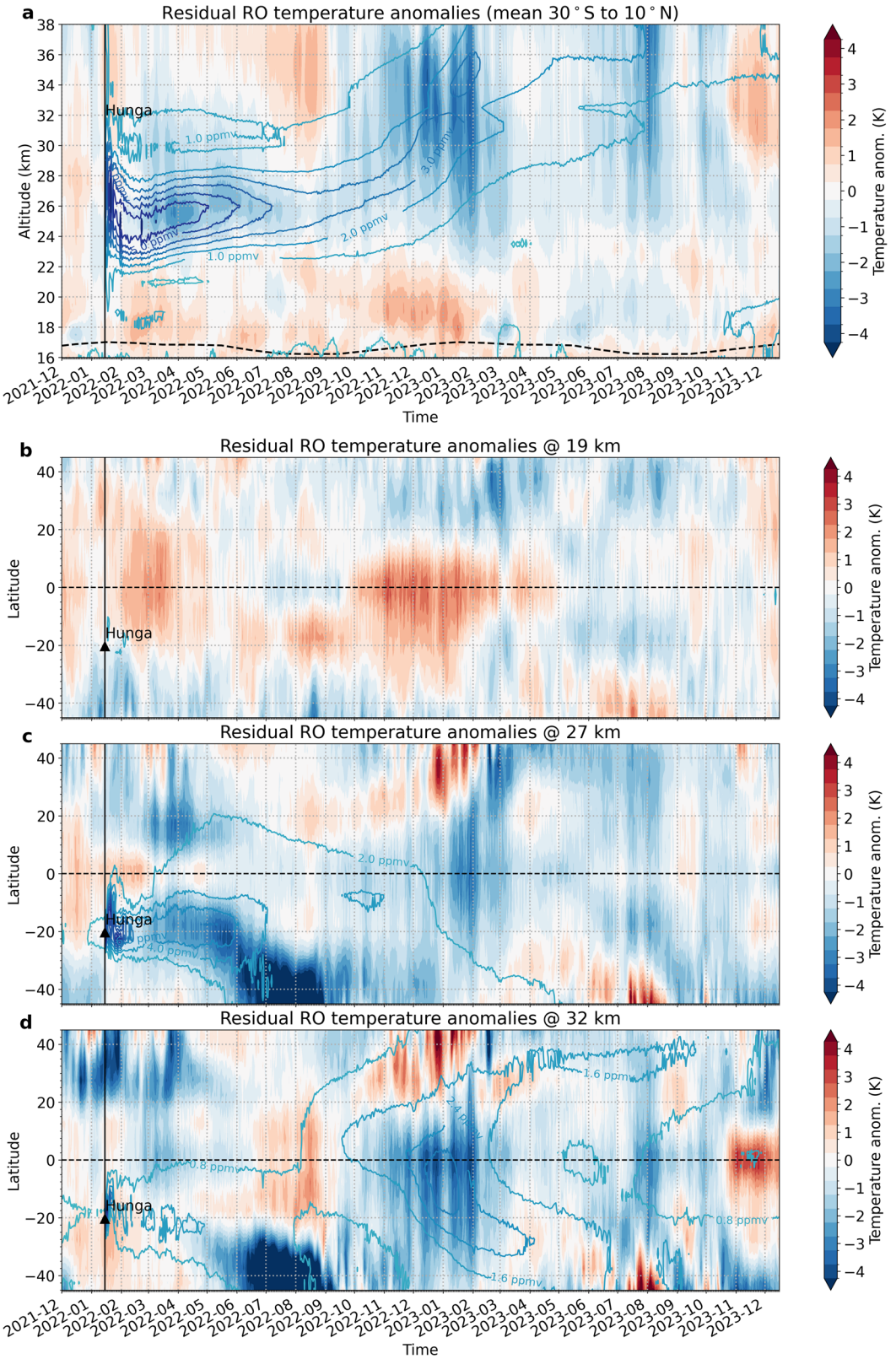

Fig. 5 | Daily residual temperature anomalies until 2 years after the Hunga eruption. Daily zonal mean RO temperature anomalies from December 2021 to December 2023, after subtracting QBO/ENSO and high latitude variability, showing the zonal mean 30°S to 10°N as function of altitude (**a**) as well as latitude slices at 19 km altitude (**b**), 27 km altitude (**c**), and at 32 km altitude (**d**). Vertical lines mark the date of the eruption. The dashed black line in (**a**) indicates the climatological lapse-rate tropopause. Contour lines in (**c**) and (**d**) show the MLS water vapor mixing ratio.

Zonal-mean temperature anomalies post-eruption

To determine longer lasting impacts of the Hunga eruption we focus on the analysis of the zonal mean temperature anomalies. We investigate the spatial distribution and temporal evolution of temperature anomalies in the stratosphere after the eruption and try to identify signals associated with the Hunga eruption against the background of strong natural variability.

Figure 2 provides an overview of the zonal mean temperature anomaly time series, giving insights into the temperature changes after the eruption until end of 2023. Figure 2a displays temperature anomalies as function of altitude in a latitude region (30°S to 10°N) affected by the volcanic plume, while Fig. 2b–d zoom in on specific altitude sections to illustrate the latitudinal structure of the temperature anomalies in the tropics and subtropics, respectively.

As can be seen in Fig. 2a, the zonal mean temperature anomalies shortly after the eruption exhibit a warming, extending from the lowermost stratosphere to an altitude of more than 30 km, while the initial temperature dipole structure co-located with the early water vapor plume is not directly visible. This can be explained by the fact that the cloud is still very localized in the first few weeks after the eruption.

Particularly strong warming can be observed in the lowermost stratosphere in the tropics and subtropics (30°S to 40°N) (Fig. 2b) and in the central tropics (10°S to 10°N), strongest at an altitude of around 27 km (Fig. 2c) immediately after and to a smaller extent also prior to the eruption. These anomalies are complemented by negative temperature anomalies at high latitudes of the Northern Hemisphere (>40°N in Fig. 2c, d), suggesting a dynamical connection (see-saw pattern) between these regions[33,34]. Another positive anomaly, which is centered in the tropical region, appears in September 2022 in the mid to lower stratosphere (Fig. 2a, b).

Upon closer examination of the wind shear (contour lines in Fig. 2a), it becomes evident that the positive anomalies observed in the mid to lower stratosphere are more likely linked to the QBO, specifically a westerly shear phase of the QBO, rather than solely attributable to the Hunga eruption.

Figure 2a also displays an unusual cooling during March 2022, not explainable by the QBO westerly shear phase which, in general, correlates with warmer conditions. In Fig. 2c, it becomes clear that this cooling, beginning at the end of February, extends across the northern and southern mid to low latitudes. In the Northern Hemisphere, the cooling can predominantly be attributed to the dynamical coupling with the northern high-latitudes, where changes in the overturning circulation lead to anti-correlated temperature anomalies between high and low latitudes (see-saw pattern)[33,34]. In the Southern Hemisphere, the cooling persists until austral winter 2022, expands toward higher latitudes, and seems to have no dynamical origin. After October 2022, strong negative temperature anomalies, which will be addressed further below, can be observed in the tropical mid and lower stratosphere (Fig. 2a, d).

The temperature patterns visible in Fig. 2 imply that natural variability partially overlaps possible eruption signatures. Thus, to accurately determine and quantify the Hunga signals, the effects of the most important variability modes must be taken into account.

Variability cleared temperature anomalies

To identify the actual impact of the Hunga eruption among the different natural variability modes, we performed a multiple linear regression analysis. Using this approach, we decompose and account for the influence of the QBO, variations in solar flux, the El Niño-Southern Oscillation (ENSO), and dynamical coupling with high latitudes (see-saw pattern)[33,34].

The reconstructed temperature anomalies associated with these natural variability modes are illustrated in Fig. 3. The QBO's westerly shear phase is evident in Fig. 3a and particularly in Fig. 3c, showing pronounced positive temperature anomalies predominantly affecting the tropics. Similarly, the QBO's easterly shear phase is apparent through negative temperature anomalies in the mid and lower stratosphere from late 2022 to early 2023, as displayed in Fig. 3a, c, d. Additionally, the reconstructed anomalies show dynamically induced see-saw signals in the mid-latitudes shortly before and after the eruption, resulting in positive temperature anomalies in the lowermost stratosphere (Fig. 3b) and pronounced negative temperature anomalies from the lower to the middle stratosphere (Fig. 3c, d).

In addition, Figs. 2a, b and 3a, b show that much of the warming in Fig. 1 in the lower stratosphere in February is the result of a large-scale circulation effect rather than being related to aerosols or water vapor.

Figure 4 displays the residual monthly mean RO-based temperature anomalies after subtracting the natural variability modes, showing the altitudes (left) and months (right) where the strongest signals related to the Hunga eruption in the tropics and subtropics are observed.

Some of the residual anomalies following the eruption are the strongest in the entire residual RO time series from January 2005 to June 2023 (Fig. 4b, c). Immediately after the Hunga eruption, the temperature residuals in the lower to middle stratosphere, especially around 27 km altitude, show a significant cooling of the southern subtropical region extending from 30°S to 15°S. While the negative anomaly in the Northern Hemisphere (c.f. Fig. 2c) is largely reduced by accounting for the dynamical coupling with high latitudes, the cooling in the Southern Hemisphere surpasses all residual anomalies observed in this region since 2005 (dashed line in Fig. 4b). The following pronounced negative anomalies of more than −6 K between 30°S and 45°S during austral winter 2022 (Fig. 4b, c) are the strongest in the whole time series[25] and can be attributed to a Hunga forced coupled effect involving water vapor and aerosols[19], which impacted stratospheric circulation and possibly polar vortex strength.

At altitudes of about 32 km and above (Fig. 4c), also the tropical stratosphere exhibits a prominent cooling from fall 2022 to early 2023 in the middle to upper tropical stratosphere. The residual temperature anomalies are outside all previous variability in the residual time series for this region and differ by more than three standard deviations in some areas.

In contrast, only insignificant warming signals remain in the lowermost tropical stratosphere (Fig. 4a) after removing temperature signatures from QBO and dynamical coupling. While the residual warming in January and February 2022 in the lowermost stratosphere is likely linked to aerosol heating[18,26], the warming starting in October corresponds to a pronounced positive ozone anomaly (Fig. S2), which is characteristic of dynamical changes[35]. This in turn indicates a slowdown of the vertical updraft of the BDC in the tropics[19,25].

Climatological impact of Hunga induced water vapor

To facilitate the interpretation of the detailed spatiotemporal development of the Hunga signals, Fig. 5 illustrates the daily residual RO temperature anomalies following the Hunga eruption after natural variability modes have been removed and relates it to the water vapor distribution.

Figure 5a displays the mean temperature anomalies within 30°S to 10°N as function of altitude. Notably, a distinct pattern emerges where negative temperature anomalies closely align with the distribution of water vapor, ascending from the lower to the mid stratosphere. A temporal interruption in the mid-2022 cooling is evident, where a positive temperature anomaly emerges in the mid stratosphere. This anomaly is associated with the Hunga forced dynamic alterations during austral winter 2022[19,25], and counterbalances the radiative cooling attributed to the water vapor from the Hunga eruption. As we progress into fall 2022, driven by prevailing strong upward winds, the water vapor plume begins to ascend further into the mid stratosphere. Consequently, a recovery of the robust cooling can be observed within an altitude range from 26 km to above 38 km.

While Fig. 5b shows that residual anomalies are small in the lowermost stratosphere, robust cooling is observable at higher altitudes. Figure 5c, d illustrates that the cooling pattern aligns closely with the latitudinal spread of the water vapor plume, which, during the first five months, is still confined within a relatively narrow latitude band ranging from 10°S to 30°S (Fig. 5c). By June 2022, the water vapor plume begins to extend toward the mid-southern latitudes, coinciding with the intense cooling observed at mid to high latitudes in the Southern Hemisphere. This indicates that the low temperatures at mid to high southern latitudes are the product of a combined effect from the strong Southern Hemisphere polar vortex and the

radiative cooling generated by the water vapor. Furthermore, as the plume ascends in the tropics starting in fall 2022, the cooling is centered between 25°S to 15°N, aligning with the latitudinal distribution of water vapor (Fig. 5d). During the entire transport process until the water vapor reaches above the mid-stratosphere, depending on latitude and altitude, the cooling ranges between −3 K and −4 K. Consistent results are found when MLS temperature data are used for the analysis (Fig. S5).

Although limitations in the regression analysis leave residual artifacts (e.g., residual anomalies at northern mid-latitudes in late 2022 and early 2023), the clear alignment of the cooling signals with water vapor distribution indicates that the negative temperature anomalies are caused by radiative cooling. This is further confirmed by Fig. S3 which excludes a pure dynamical cause for the months with strong Hunga signals.

Discussion

Our analysis provides an overview on the observed impact of the Hunga volcanic plume on stratospheric temperature, utilizing GNSS RO and MLS measurements. We address the temporal evolution of temperature anomalies and their relationship with the distribution of water vapor following the eruption. Furthermore, our results demonstrate consistency between RO and MLS temperature measurements soon after the eruption and also highlight the potential of RO for climate analysis following extreme events such as volcanic eruptions.

The eruption of the Hunga volcano in early 2022 resulted in significant stratospheric temperature perturbations, observed shortly after the event and lasting for more than 1 year until the water vapor was transported above the mid stratosphere. Alongside eruption-related signals, natural variability modes such as the QBO in the equatorial region and dynamic coupling with high latitude variability are evident. The interpretation of the Hunga related signals necessitates careful consideration of natural variability modes manifesting on different time scales. We made an effort to separate this background variability from Hunga forced signals using multiple linear regression analysis.

Our results reveal a substantial and persistent impact of the Hunga eruption on the thermal structure of the stratosphere. This is evident through several key findings.

Shortly after the eruption, a temperature dipole following the altitudinal evolution of the water vapor with a cooling above and a warming below the maximum water vapor can be observed. While the RO data overestimate the dipole structure in the first days after the eruption due to the extreme amount of water vapor, the dipole structure also becomes clearly visible in the MLS temperature measurements.

A dipole structure has also been simulated in model studies using the Whole Atmosphere Community Climate Model (WACCM), where it is primarily attributed to long-wave forcing considering the effect of water vapor and aerosols[19]. A comparison between the model simulations and our observational data shows considerable agreement, although the WACCM simulations find the maximum cooling at the level of the water vapor maximum, while the observations show cooling above this level. This discrepancy suggests that additional processes are at play which might not be captured by the WACCM model[19], especially within the early plume where aerosols and water vapor are mixed.

The localized cooling immediately after the eruption is followed by a widespread cooling in the lower tropical and subtropical stratosphere which starts in mid-February 2022 and closely aligns with the distribution of the water vapor.

Figure 5 clearly highlights that radiative cooling by water vapor is the primary driver for the observed negative temperature anomalies in the tropics and subtropics between February 2022 and March 2023. This is also the case for the extraordinarily strong negative anomaly of approximately −4 K that manifests in the tropical mid-stratosphere in late 2022 and early 2023. After accounting for natural variability, these anomalies are the strongest in the tropical and subtropical middle and lower stratosphere throughout the whole time series starting in 2005.

In contrast, we do not find temperature signals that are obviously related to the aerosol plume (Fig. S4). However, aerosols could play a role for the positive temperature anomalies observed in the lowermost stratosphere immediately after the eruption.

Model simulations show that some of the temperature anomalies, such as the cooling at high southern latitudes and the associated warming in the tropical mid-stratosphere between June and October 2022, also have a dynamical component as the Hunga eruption has impacted the BDC and the strength of the polar vortex[19,25]. The persistent water vapor in the middle stratosphere and the associated continued cooling in the tropics until March 2023 could also have influenced the upwelling of the BDC.

In our study we highlight the complex entanglement between eruption-induced anomalies and natural modes of variability. We demonstrate the importance of distinguishing the Hunga signals from dominant stratospheric variability modes to accurately assess their impact. Therefore, our documentation of observed Hunga induced temperature changes will be useful for future modeling analyses, as they provide a benchmark for testing simulation results against observational analyses.

Data and methods

Analyzing the temperature anomaly profiles within the early volcanic plume

To analyze the temperature variations within the early volcanic plume we use level 2 near real-time (NRT) dry temperature profiles obtained from COSMIC-2[27], Spire[28] and PlanetIQ GNSS RO measurements, together with water vapor and temperature recorded by the MLS instrument onboard the Aura satellite[29–31]. MLS/Aura Level 2 Version 4 water vapor and temperature data are binned to a regular 2.5° × 2.5° latitude/longitude grid with daily resolution. We apply standard quality screening criteria[36] for MLS temperature data, whereas adjusted quality screening criteria are employed for water vapor data to prevent misclassification of the exceptionally high mixing ratios induced by the Hunga volcano[16]. GNSS RO profiles were processed by the COSMIC Data Analysis and Archive Center (CDAAC) at the University Corporation for Atmospheric Research (UCAR). Only RO profiles flagged as high quality are used for the analysis.

RO data provide accuracy, global coverage, and high vertical resolution within the UTLS region[37–39]. RO measurements can hold intrinsic information of temperature and water vapor in case of a moist atmosphere. In a dry atmosphere, as usually prevails in the UTLS, water vapor is negligible, and temperature is retrieved directly from bending angle and refractivity. We use "dry temperature", which is very close to the physical temperature in the UTLS[40,41]. The physical temperature, which combines measurement and background data, is more suitable for the lower troposphere, where humidity plays an important role.

However, as RO dry temperature profiles can be influenced by extremely high amounts of stratospheric water vapor, we cross checked the results from RO against the MLS temperature measurements (see Supplementary Fig. S5).

First, we select a latitude band from 40°S to 25°N where the water vapor plume is located. Within this region, we select RO profiles for which one of the neighboring gridpoints in the gridded daily MLS water vapor data has a mixing ratio greater than 80% of the maximum mixing ratio for that day. From these RO profiles, we then compute temperature anomaly profiles. We construct a 2.5° × 2.5° latitude/longitude reference climatology (2005 to 2021) and subtract the climatological profile of the nearest RO gridpoint for the corresponding month from the individual profile. Similarly for MLS we use those temperature gridpoints that coincide with the selected MLS water vapor gridpoints. MLS temperature anomalies are computed by subtracting the corresponding MLS climatology (2005 to 2021).

For creation of the reference climatology for the RO profiles, we use profile data processed by the Radio Occultation Meteorology Satellite Application Facility (ROM SAF)[42], while a monthly temperature climatology was created for the MLS data. A similar methodology has previously been used successfully to describe vertical thermal structures during tropical cyclones and after volcanic eruptions[43].

Accounting for natural variability modes

To distinguish the temperature signals caused by the Hunga eruption from the different natural variability patterns, we use a multiple linear regression analysis considering autocorrelation with a generalized least squares model accounting for autocorrelated AR(1) errors. In order to properly represent and account for slowly varying modes of variability such as the QBO and ENSO, we base the analysis on a multi-year time series for the period January 2005 to June 2023.

In a first step, monthly mean temperatures on 5°-latitude bands and a vertical grid of 500 m are generated from the RO data. The gridded ROM SAF RO dataset extends until December 2022 and is extended with the COSMIC-2, Spire and PlanetIQ NRT data through December 2023. We then subtract the mean seasonal cycle from the data using the time series from January 2005 to December 2021 as reference climatology.

Several indices are used to account for different natural modes of variability. The QBO is accounted for with indices derived from the Singapore wind field by empirical orthogonal function (EOF) analysis[44], where we use the three leading EOFs. The impact of the ENSO is accounted for via the Niño 3.4 sea surface temperature (SST) index with a three-month lag. In addition, we create indices that represent the dynamic coupling between high latitudes and the tropics and subtropics[33,34]. These indices consist of monthly mean temperatures for specific latitude bands averaged over 65°N to 90°N for the Northern Hemisphere and 65°S to 90°S for the Southern Hemisphere. The use of monthly means is suitable for representing QBO and ENSO and also a substantial part of the dynamical coupling with the high latitudes. However, rapid fluctuations in high latitude variability might not be fully covered.

Using these variability indices, we perform the regression analysis. With the resulting regression coefficients we reconstruct temperatures attributable to the different variability modes. The reconstructed temperatures are then subtracted from the deseasonalized monthly temperature anomalies.

We also subtract the monthly reconstructed temperature fields for the variability modes and the seasonal cycle from the daily gridded RO NRT data from December 2021 to December 2023. For this purpose, we converted the monthly seasonal cycle and reconstructed variability fields into daily values by linear interpolation, setting the monthly value to the central day of the month. Although a full consideration of the natural variability is not possible, the remaining anomalies consist mainly of random variations and changes due to the Hunga eruption.

Data availability

The GNSS RO COSMIC-2, Spire and PlanetIQ Near Real Time (NRT) data used in this study are available through the COSMIC Data Analysis and Archive Center (CDAAC)[45] website (https://data.cosmic.ucar.edu/gnss-ro/). GNSS RO temperature data used for the climatology can be obtained from the ROM SAF[46] (https://doi.org/10.15770/EUM_SAF_GRM_0001). The El Niño-Southern Oscillation (ENSO) and Quasi-biennial Oscillation (QBO) data used in the regression analysis were downloaded from the National Weather Service Climate Prediction Center (CPC) (https://www.cpc.ncep.noaa.gov/data/indices/ersst5.nino.mth.81-10.ascii) and NASA/GSFC data services (https://acd-ext.gsfc.nasa.gov/Data_services/met/qbo/qbo.html), respectively. MLS temperature[47], water vapor[48] and ozone[49] data were obtained from the NASA Goddard Earth Sciences Data and Information Services Center (GES DISC) website (https://doi.org/10.5067/Aura/MLS/DATA2021, https://doi.org/10.5067/Aura/MLS/DATA2009 and https://doi.org/10.5067/Aura/MLS/DATA2017 (accessed on 17 August 2023)). OMPS-LP Level 2 aerosol data were obtained from the University of Saskatchewan (https://research-groups.usask.ca/osiris/data-products.php#OSIRISLevel2DataProducts (accessed on 3 May 2024)). Processed data[50] are available at Zenodo (https://doi.org/10.5281/zenodo.12682814).

Code availability

The analysis was performed in Python using statsmodels (version 0.14.0), Xarray, pandas, and others. Scripts are available on Zenodo at https://doi.org/10.5281/zenodo.12697984.

Received: 17 January 2024; Accepted: 7 August 2024;
Published online: 21 August 2024

References

1. Maycock, A. C. et al. Revisiting the mystery of recent stratospheric temperature trends. *Geophys. Res. Lett.* **45**, 9919–9933 (2018).
2. Yu, P. et al. Persistent stratospheric warming due to 2019–2020 Australian wildfire smoke. *Geophys. Res. Lett.* **48**, e2021GL092609 (2021).
3. Stocker, M., Ladstädter, F. & Steiner, A. K. Observing the climate impact of large wildfires on stratospheric temperature. *Sci. Rep.* **11**, 22994 (2021).
4. Baldwin, M. P. et al. Sudden stratospheric warmings. *Rev. Geophys.* **59**, e2020RG000708 (2021).
5. Robock, A. Volcanic eruptions and climate. *Rev. Geophys.* **38**, 191–219 (2000).
6. Kremser, S. et al. Stratospheric aerosol—observations, processes, and impact on climate. *Rev. Geophys.* **54**, 278–335 (2016).
7. Stocker, M., Ladstädter, F., Wilhelmsen, H. & Steiner, A. K. Quantifying stratospheric temperature signals and climate imprints from post-2000 volcanic eruptions. *Geophys. Res. Lett.* **46**, 12486–12494 (2019).
8. Proud, S. R., Prata, A. T. & Schmauß, S. The January 2022 eruption of Hunga Tonga-Hunga Ha'apai volcano reached the mesosphere. *Science* **378**, 554–557 (2022).
9. Matoza, R. S. et al. Atmospheric waves and global seismoacoustic observations of the January 2022 Hunga eruption, Tonga. *Science* **377**, 95–100 (2022).
10. Millán, L. et al. The Hunga Tonga-Hunga Ha'apai Hydration of the Stratosphere. *Geophys. Res. Lett.* **49**, e2022GL099381 (2022).
11. Carn, S. A., Krotkov, N. A., Fisher, B. L. & Li, C. Out of the blue: volcanic SO2 emissions during the 2021–2022 eruptions of Hunga Tonga—Hunga Ha'apai (Tonga). *Front. Earth Sci.* **10** (2022).
12. Legras, B. et al. The evolution and dynamics of the Hunga Tonga–Hunga Ha'apai sulfate aerosol plume in the stratosphere. *Atmos. Chem. Phys.* **22**, 14957–14970 (2022).
13. Khaykin, S. et al. Global perturbation of stratospheric water and aerosol burden by Hunga eruption. *Commun. Earth Environ.* **3**, 316 (2022).
14. Sellitto, P. et al. The unexpected radiative impact of the Hunga Tonga eruption of 15th January 2022. *Commun. Earth Environ.* **3**, 288 (2022).
15. Zhu, Y. et al. Perturbations in stratospheric aerosol evolution due to the water-rich plume of the 2022 Hunga-Tonga eruption. *Commun. Earth Environ.* **3**, 248 (2022).
16. Xu, J., Li, D., Bai, Z., Tao, M. & Bian, J. Large amounts of water vapor were injected into the stratosphere by the Hunga Tonga–Hunga Ha'apai volcano eruption. *Atmosphere* **13**, 912 (2022).
17. Randel, W. J. et al. Stratospheric water vapor from the Hunga Tonga–Hunga Ha'apai volcanic eruption deduced from COSMIC-2 radio occultation. *Remote Sens.* **15**, 2167 (2023).
18. Schoeberl, M. R. et al. Analysis and impact of the Hunga Tonga-Hunga Ha'apai stratospheric water vapor plume. *Geophys. Res. Lett.* **49**, e2022GL100248 (2022).
19. Wang, X. et al. Stratospheric climate anomalies and ozone loss caused by the Hunga Tonga-Hunga Ha'apai volcanic eruption. *J. Geophys. Res. Atmos.* **128**, e2023JD039480 (2023).
20. Santee, M. L. et al. Strong evidence of heterogeneous processing on stratospheric sulfate aerosol in the extrapolar Southern Hemisphere following the 2022 Hunga Tonga-Hunga Ha'apai eruption. *J. Geophys. Res. Atmos.* **128**, e2023JD039169 (2023).
21. Wilmouth, D. M., Østerstrøm, F. F., Smith, J. B., Anderson, J. G. & Salawitch, R. J. Impact of the Hunga Tonga volcanic eruption on stratospheric composition. *Proc. Natl Acad. Sci.* **120**, e2301994120 (2023).

22. Dunn, R. J. H. et al. Global climate. *Bull. Am. Meteorol. Soc.* **104**, S11–S145 (2023).
23. Jenkins, S., Smith, C., Allen, M. & Grainger, R. Tonga eruption increases chance of temporary surface temperature anomaly above 1.5 °C. *Nat. Clim. Change* **13**, 127–129 (2023).
24. Fleming, E. L., Newman, P. A., Liang, Q. & Oman, L. D. Stratospheric temperature and ozone impacts of the Hunga Tonga-Hunga Ha'apai water vapor injection. *J. Geophys. Res. Atmos.* **129**, e2023JD039298 (2024).
25. Coy, L. et al. Stratospheric circulation changes associated with the Hunga Tonga-Hunga Ha'apai eruption. *Geophys. Res. Lett.* **49**, e2022GL100982 (2022).
26. Vömel, H., Evan, S. & Tully, M. Water vapor injection into the stratosphere by Hunga Tonga-Hunga Ha'apai. *Science* **377**, 1444–1447 (2022).
27. Schreiner, W. S. et al. COSMIC-2 radio occultation constellation: first results. *Geophys. Res. Lett.* **47**, e2019GL086841 (2020).
28. Jing, X. et al. Spire RO thermal profiles for climate studies: initial comparisons of the measurements from spire, NOAA-20 ATMS, Radiosonde, and COSMIC-2. *Remote Sens.* **15**, 3710 (2023).
29. Waters, J. W. et al. The Earth observing system microwave limb sounder (EOS MLS) on the aura Satellite. *IEEE Trans. Geosci. Remote Sens.* **44**, 1075–1092 (2006).
30. Schwartz, M. J. et al. Validation of the Aura Microwave Limb Sounder temperature and geopotential height measurements. *J. Geophys. Res. Atmos.* **113**, D15S11 (2008).
31. Read, W. G. et al. Aura microwave limb sounder upper tropospheric and lower stratospheric H2O and relative humidity with respect to ice validation. *J. Geophys. Res. Atmos.* **112** (2007).
32. Carr, J. L., Horváth, Á., Wu, D. L. & Friberg, M. D. Stereo plume height and motion retrievals for the record-setting Hunga Tonga-Hunga Ha'apai eruption of 15 January 2022. *Geophys. Res. Lett.* **49**, e2022GL098131 (2022).
33. Yulaeva, E., Holton, J. R. & Wallace, J. M. On the cause of the annual cycle in tropical lower-stratospheric temperatures. *J. Atmos. Sci.* **51**, 169–174 (1994).
34. Rieger, L. A., Randel, W. J., Bourassa, A. E. & Solomon, S. Stratospheric temperature and ozone anomalies associated with the 2020 Australian New Year Fires. *Geophys. Res. Lett.* **48**, e2021GL095898 (2021).
35. Randel, W. J., Wu, F., Ming, A. & Hitchcock, P. A simple model of ozone–temperature coupling in the tropical lower stratosphere. *Atmos. Chem. Phys.* **21**, 18531–18542 (2021).
36. Livesey, N. J. et al. Technical Report, Version 4.2x Level 2 and 3 data quality and description document. https://mls.jpl.nasa.gov/data/v4-2_data_quality_document.pdf (2020).
37. Steiner, A. K. et al. GPS radio occultation for climate monitoring and change detection. *Radio Sci.* **46**, RS0D24 (2011).
38. Steiner, A. K. et al. Consistency and structural uncertainty of multi-mission GPS radio occultation records. *Atmos. Meas. Tech.* **13**, 2547–2575 (2020).
39. Scherllin-Pirscher, B., Kirchengast, G., Steiner, A. K., Kuo, Y.-H. & Foelsche, U. Quantifying uncertainty in climatological fields from GPS radio occultation: an empirical-analytical error model. *Atmos. Meas. Tech.* **4**, 2019–2034 (2011).
40. Danzer, J., Foelsche, U., Scherllin-Pirscher, B. & Schwärz, M. Influence of changes in humidity on dry temperature in GPS RO climatologies. *Atmos. Meas. Tech.* **7**, 2883–2896 (2014).
41. Scherllin-Pirscher, B. et al. Tropical temperature variability in the UTLS: new insights from GPS radio occultation observations. *J. Clim.* **34**, 2813–2838 (2021).
42. Gleisner, H., Lauritsen, K. B., Nielsen, J. K. & Syndergaard, S. Evaluation of the 15-year ROM SAF monthly mean GPS radio occultation climate data record. *Atmos. Meas. Tech.* **13**, 3081–3098 (2020).
43. Biondi, R., Ho, S.-P., Randel, W., Syndergaard, S. & Neubert, T. Tropical cyclone cloud-top height and vertical temperature structure detection using GPS radio occultation measurements. *J. Geophys. Res. Atmos.* **118**, 5247–5259 (2013).
44. Hannachi, A., Jolliffe, I. T. & Stephenson, D. B. Empirical orthogonal functions and related techniques in atmospheric science: a review. *Int. J. Climatol.* **27**, 1119–1152 (2007).
45. CDAAC, CDAAC GNSS Radio Occultation Datasets. UCAR COSMIC Program. https://www.cosmic.ucar.edu/what-we-do/data-processing-center/data (2024).
46. ROM-SAF, Radio Occultation Reprocessed Climate Data Record—Multimission. EUMETSAT SAF on radio occultation meteorology. https://doi.org/10.15770/EUM_SAF_GRM_0001 (2021).
47. Schwartz, M., Livesey, N. & Read, W. MLS/Aura Level 2 Temperature V004. Goddard Earth Sciences Data and Information Services Center (GES DISC). https://doi.org/10.5067/Aura/MLS/DATA2021 (2015).
48. Lambert, A., Read, W. & Livesey, N. MLS/Aura Level 2 Water Vapor (H2O) Mixing Ratio V004. Goddard Earth Sciences Data and Information Services Center (GES DISC). https://doi.org/10.5067/Aura/MLS/DATA2009 (2015).
49. Schwartz, M., Froidevaux, L., Livesey, N. & Read, W. MLS/Aura Level 2 Ozone (O3) Mixing Ratio V004. Goddard Earth Sciences Data and Information Services Center (GES DISC). https://doi.org/10.5067/Aura/MLS/DATA2017 (2015).
50. Stocker, M. Datasets related to the paper Stocker et al. (2024), Strong persistent cooling of the stratosphere after the Hunga eruption [Data set]. Zenodo. https://doi.org/10.5281/zenodo.12682814 (2024).

Acknowledgements

M.S. and A.K.S. sincerely thank the UCAR/COSMIC team for hosting and supporting their research stays during summer 2023 within the UCAR UCP and COSMIC Program in Boulder, CO, USA. M.S., F.L., A.K.S. and U.F. were funded by the University of Graz, Graz, Austria. We acknowledge the use of imagery from the NASA Worldview application (https://worldview.earthdata.nasa.gov), part of the NASA Earth Science Data and Information System (ESDIS).

Author contributions

A.K.S., W.J.R. and M.S. designed the study. M.S. collected the data, performed the analysis, created the figures and wrote the initial manuscript. F.L. contributed substantially to data processing and analysis. All authors discussed the results and their implications and contributed to figure design and writing of the manuscript at all stages. A.K.S., U.F. and W.J.R. provided guidance and advise on all aspects of the study.

Competing interests

The authors declare no competing interests.

Additional information

Supplementary information The online version contains supplementary material available at https://doi.org/10.1038/s43247-024-01620-3.

Correspondence and requests for materials should be addressed to Matthias Stocker.

Peer review information *Communications Earth & Environment* thanks the anonymous reviewers for their contribution to the peer review of this work. Primary Handling Editors: Sylvia Sullivan and Heike Langenberg. A peer review file is available.